Effects of electron-phonon interactions on the electron tunneling spectrum of PbS quantum dots

Hongjian Wang, Emmanuel Lhuillier, Q Yu, A Mottaghizadeh, C Ulysse, A Zimmers, A Descamps-Mandine, Benoit Dubertret, Herve Aubin

Effects of electron-phonon interactions on the electron tunneling spectrum of PbS quantum dots

H. Wang,[1,2,3] E. Lhuillier,[1,2,3] Q. Yu,[1,2,3] A. Mottaghizadeh,[1,2,3]
C. Ulysse,[4] A. Zimmers,[1,2,3] A. Descamps-Mandine,[1,2,3] B. Dubertret,[1,2,3] and H. Aubin[1,2,3,*]

[1] *LPEM, PSL Research University, ESPCI-ParisTech, 10 rue Vauquelin, F-75231 Paris Cedex 5, France*
[2] *CNRS, UMR 8213, F-75005 Paris, France*
[3] *Sorbonne Universités, UPMC Univ Paris 06, F-75005 Paris, France*
[4] *Laboratoire de Photonique et de Nanostructures, CNRS, 91460 Marcoussis, France*

(Dated: January 29, 2015)

We present a tunnel spectroscopy study of single PbS Quantum Dots (QDs) as function of temperature and gate voltage. Three distinct signatures of strong electron-phonon coupling are observed in the Electron Tunneling Spectrum (ETS) of these QDs. In the shell-filling regime, the 8× degeneracy of the electronic levels is lifted by the Coulomb interactions and allows the observation of phonon sub-bands that result from the emission of optical phonons. At low bias, a gap is observed in the ETS that cannot be closed with the gate voltage, which is a distinguishing feature of the Franck-Condon (FC) blockade. From the data, a Huang-Rhys factor in the range $S \sim 1.7 - 2.5$ is obtained. Finally, in the shell tunneling regime, the optical phonons appear in the inelastic ETS d^2I/dV^2.

PACS numbers: 81.30.Bx, 71.30.+h, 73.21.-b,73.22.-f

Semiconducting nanocrystals are characterized by discrete electronic levels with size-tunable energies[1], giving these QDs unique optical and electronical properties[2–4]. They are attractive materials for applications in solution-processable devices such as Light Emitting Diodes (LED)[5] or Field-Effect Transistors (FET) [3].

While optical absorption spectroscopy and fluorescence spectroscopy are usually employed to characterize the properties of isolated QDs, the ETS is a more relevant characterization when the goal is to incorporate the QDs into electron conducting devices such as FET or LED. Indeed, the coupling of a QD to electrodes or neighboring QDs, in presence of Coulomb and electron-phonon interactions, strongly alters the electronic spectrum of the QD and, consequently, the electronic transmission coefficient of the QD.

In this work, we have studied the ETS of PbS QDs. Lead chalcogenides feature a narrow band gap in the mid-infrared and small electron and hole effective masses. As a result, the QDs made of these materials are characterized by strong quantum confinement and a size-tunable band gap on a wide energy range, which is of interest for solar cells [6–9] and infra-red detectors[10].

We have found multiple signatures of strong electron-phonon coupling in the ETS. The low energies optical phonons appear in the inelastic ETS d^2I/dV^2, phonon sub-bands appear in the elastic ETS dI/dV and a FC blockade induced by this strong electron-phonon coupling is observed at low bias. This last observation implies that using QDs with low electron-phonon coupling should help improving electronic transport in QDs thin films.

.

The PbS QDs, shown on the TEM picture Fig. 1a, are synthesized according to the procedure described in Ref.[11] and summarized in the supplementary information. After their synthesis, the organic ligands at the surface of the QDs are replaced by short inorganic ligands, S^{2-}[10, 12], to reduce the thickness of the insulating tunnel barrier between the QD and the electrodes.

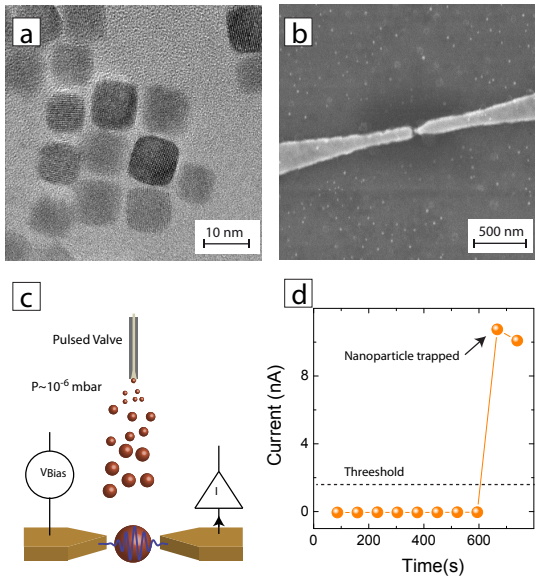

FIG. 1. a) TEM image of PbS QDs. b) SEM image of ∼ 10 *nm* spaced electrodes in which a QD has been deposited. c) Schematic of the nanofabrication process. Nanoparticles are projected onto the chip-circuit in high vacuum using a fast pulsed valve. d) After each projection, the tunnel current is measured. When it exceeds the threshold, the projection stops.

To measure the ETS as function of temperature and carrier filling, we employed on-chip tunneling spectroscopy where the nanoparticle is trapped within a nanogap, i.e. two electrodes separated by a distance about 10 nm, deposited on a p-doped silicon substrate used as a back-gate covered by a silicon oxide layer 300 nm thick. Scanning Tunneling Microscopy (STM) has already been employed to study the ETS of colloidal InAs QDs[13–15], strain-induced InAs[16], colloidal InSb[17], PbSe[18], CdSe[19–21] and PbS[22] QDs as well as electrochemically grown PbS and PbSe QDs[23]; however, on-chip tunneling spectroscopy has been only employed a few times[24–26] although this method presents several advantages. The junctions are highly stable at low temperature, which allows high resolution measurements of the elastic and inelastic ETS. Furthermore, a back gate can be implemented, which allows changing the carrier filling of the QD.

Progresses with on-chip tunneling spectroscopy have been hampered by the difficulty in fabricating single nanoparticle junctions. To that end, we developed a new method where the nanoparticle is trapped within the nanogap by directing a nanoparticle beam in vacuum onto the chip circuit as described previously[26, 27]. The chip contains 32 nanogaps and the electrodes are fabricated by standard ebeam lithography, thermal evaporation of gold and lift-off, shown on the SEM image, Fig. 1b.

To trap the QDs within the nanogap, the chip is maintained in high vacuum, 10^{-6} mbar, and the QDs are projected through a fast pulsed valve, Fig. 1c. After each projection, where a small amount of QDs is deposited, the tunnel current is measured to check for the presence of a QD. The projection is repeated hundred of times until a QD is detected. This generates a *projection curve*, Fig. 1d, where the tunnel current is zero until a QD gets trapped within the nanogap which leads to a sharp increase of the tunnel current that stops the projection system. In past works by other groups[24, 25], the nanoparticles were deposited within the nanogap in solution where the tunnel current cannot be measured. As the trapping is essentially a random process, this required the fabrication of hundred of junctions. In comparison, the projection technique described here has significant advantages. First, because the sample is fabricated in high vacuum, the tunnel current can be measured during the projection of the nanoparticles. Second, the method allows hundreds of trials i.e. projection-measure, in a few hours, which increase significantly the probability of fabricating single nanoparticle devices. 10 chips circuits have been fabricated and measured from $T = 300$ K to $T = 4.2$ K. The projection setup, as well as the cryofree cryostat employed for measurements, are implemented in a glove box under argon. Thus, after fabrication, the sample can be kept free from oxidation. The current-voltage I-V curves are measured with standard voltage sources and current amplifier. A lock-in is used to add an AC component to the DC voltage, the first harmonic of the tunnel current provides the ETS dI/dV, the second harmonic provides the inelastic ETS d^2I/dV^2. The data for three samples, A, B and C, are shown in this letter.

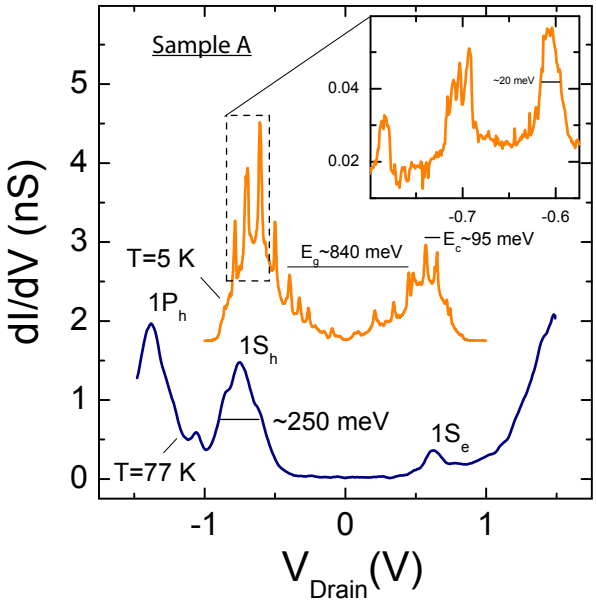

FIG. 2. dI/dV for sample A. The curve at $T = 77$ K shows the main excited levels $1S_h$, $1P_h$ and $1S_e$. The curve at $T = 5$ K shows that the degeneracy of the excited levels has been lifted by the Coulomb interactions and give rises to Coulomb peaks. The inset is a zoom on the Coulomb peaks showing that their width, ~ 20 meV, is larger than thermal smearing ~ 0.45 meV.

Figure 2 shows the dI/dV curves measured on sample A at two different temperatures. At the highest temperature, $T = 77$ K, the curve shows conductance peaks corresponding to the excited hole levels $1S_h$, $1P_h$ and electron level $1S_e$ of the QD.

At the lower temperature, $T = 5$ K, the ETS is modulated by sharp conductance peaks which are characteristics Coulomb blockade peaks in the shell filling regime[28]. In this regime, the tunneling rate Γ_{in} for electrons entering the QD is larger than the tunneling rate Γ_{out} for electrons escaping the QD. From the voltage separation between two peaks, we obtain the value $E_c \sim 95$ meV for the Coulomb energy.

This experimental value is consistent with the calculated Coulomb energy $E_c = e^2/C_{self}$ where $C_{self} = r/(1/\kappa_m + 0.79/\kappa_{PbS})$ is the self-capacitance of the QD, using for the diameter $2\times r \sim 8.5$ nm, $\kappa_m = 4\pi\varepsilon_m\varepsilon_0$ with $\varepsilon_m = 1.8$, which is the average dielectric coefficient of the media surrounding the QD, and $\kappa_{PbS} = 4\pi\varepsilon_{PbS}\varepsilon_0$ where $\varepsilon_{PbS} = 170$ is the static dielectric coefficient of PbS.

From these parameters, we also obtain the polarisation energy[29–31], $\Sigma \sim 95$ meV. As the excitation gap E_{g0}

is related to the tunneling gap E_g through the relation $E_g = E_{g0} + 2\Sigma$, one find the experimental value $E_{g0} \sim 640$ meV at $T = 5\ K$. This value is consistent with the excitation gap expected from **k.p** four bands envelope function formalism[32].

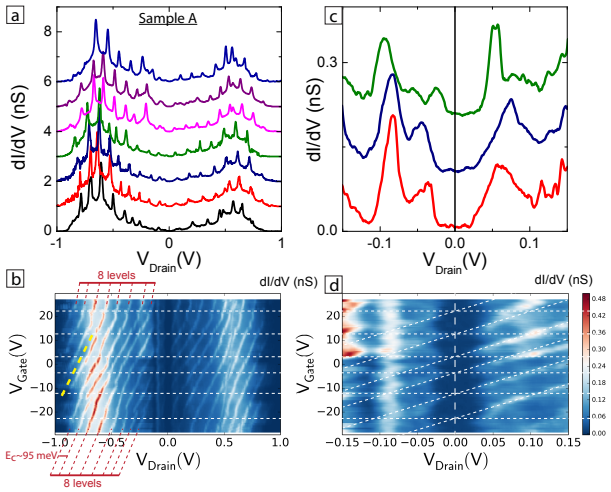

FIG. 3. dI/dV curves for sample A, plotted on panel (a) for $V_{Gate} = -27, -17, -7, 0, 7, 17, 27$ V and shown on the color plot (b) as function of drain and gate voltage. The red dashed lines highlight the eight Coulomb peaks of the $1S_h$ excited level. The yellow dashed line is used to calculate the back-gate lever arm α_C. Zoom on the dI/dV curves at low drain bias, from $V_{Drain} = -0.15$ V to $V_{Drain} = +0.15$ V, plotted on panel (c) for $V_{Gate} = -17, -7, 0$ V and shown on the color plot (d). The white horizontal dashed lines highlight the gate voltage where the number of electron in the QD is changed by one. This zoom shows that the gap at low bias cannot be lifted by the gate voltage. On panels a) and c), the curves have been displaced for clarity.

Because PbS has the rock-salt crystal structure and, as a result, has direct band gaps at four equivalent L points in the Brillouin zone[32], the excited levels $1S_e$ and $1S_h$ are 8 times degenerated, after taking into account the spin degeneracy. In the shell-filling regime, this implies that up to 8 peaks separated by the Coulomb energy should be observed in the conductance curves. Fig. 3a shows the dI/dV curves for sample A as function of gate voltage, shown on the color plot Fig. 3b. At any gate voltage, exactly 8 conductance peaks can be clearly distinguished as function of drain voltage. This implies that the injected electrons are indeed populating the $1S_e$ and $1S_h$ levels of the QD. The fact that excitations occur primarily in one direction is due to asymmetric tunnel barriers[33]. Fig. 3b shows that the Coulomb peaks are shifted with the gate bias and eventually cross zero-energy, where the number of electrons in the QD changes by one, and leads to the apparition of Coulomb diamonds, as shown on the zoom at low bias, Fig. 3d. Such behavior was also observed for sample B, shown Fig. 4. For this sample, the Coulomb energy $E_c \sim 50$ meV and so the QD diameter is $2 \times r \sim 16$ nm. Because of this larger diameter, excitations levels are broad and not clearly apparent for this sample. However, as seen below, this sample allows observing clear phonon sub-bands.

Before turning to this, a few remarks are in order. The calculated capacitance between a sphere of radius r and a metallic plane at the gate distance $d = 300$ nm gives $C_{sp}/e = 5.3\ \mathrm{V}^{-1}$ for sample A and $C_{sp}/e = 10.2\ \mathrm{V}^{-1}$ for sample B[31]. We find for the experimental values $C/e = 0.1\ \mathrm{V}^{-1}$ for sample A and $C/e = 2.5\ \mathrm{V}^{-1}$ for sample B. These values are smaller than the theoretical value because of the screening effects due to the electrodes, which depends on the exact position of the QD with respect to the electrodes. One can see, for sample A, that the back-gate lever arm is different for the Coulomb and the excited levels ($1S_e$,$1S_h$). While the lever arm for the Coulomb peak is $\alpha_C = \delta E_c/\delta V_{Gate} \sim 0.0085$, the excitation peaks are barely shifting with the gate. This can be understood as a consequence of the good screening properties of PbS which has a large static dielectric coefficient. This effect will be the subject of another publication and is not important for the present discussion on the electron-phonon coupling. Finally, the observation of Coulomb diamonds is usually expected in metallic nanoparticules or in semiconducting QDs where the Fermi level has been driven in the conductance or valence bands with the gate voltage. Even if the applied gate voltage is not sufficient to push the excited levels across zero bias, the broadening of excited levels is sufficient to produce a residual density of states within the semiconducting gap, allowing the QD to effectively behave as a metallic nanoparticle. This is consistent with the recent STM observation of midgap states in PbS QDs[22] and transport measurements in PbS QDs thin films[34].

As we have seen, the degeneracy lifting effect of the Coulomb energy is the main origin for the broad peak observed Fig. 2. However, the inset of Fig. 2 shows that a single Coulomb peak has a width ~ 20 meV which is still much broader than the thermal smearing at $T = 5$ K. Similar broadening were observed in STM spectra on CdSe[21] and PbS[22].

A zoom at the Coulomb peaks measured on sample B, Fig. 4, clearly shows that the Coulomb peak is constituted of sub-bands separated by an energy of ~ 8 meV. These peaks can also be observed for sample A, but with lower resolution. These peaks are equally spaced and strongly resemble the expected response when the electron level is coupled to phonon modes[2, 35, 36]. This behavior has been observed previously in STM spectroscopy of CdSe QDs[21] in molecules[37–39] and nanotubes based QDs[40, 41].

The coupling of electronic levels with vibrational modes can be described in terms of the FC model[2, 35, 36]. In the case of a single phonon mode $\hbar\omega_0$, the FC theory gives for the transition probability :

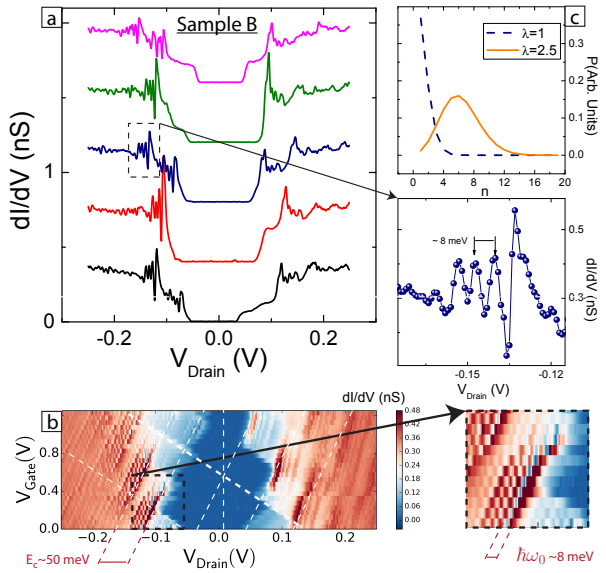

FIG. 4. dI/dV curves for sample B, plotted on panel (a) from $V_{Gate} = 0$ V to $V_{Gate} = 1.2$ V and shown on the color plot (b) as function of drain and gate voltage. These panels show that the gap at low bias cannot be lifted by the gate bias. The zoom on the dI/dV curve at $V_{Gate} = 0.4\ V$ and the zoom on the color plot show that a single Coulomb peak is formed of phonon sub-bands separed by the phonon energy $\hbar\omega_0 \sim 8$ meV. (c) Theoretical amplitude, Eq. 1, of the FC peaks as function of the number of emitted phonons for two values of the Huang-Rhys factor $\lambda = 1$ (dashed line) and $\lambda = 2.5$ (continuous line). At large λ, the matrix element goes to zero for small n, indicating the FC blockade.

$$X_{0n}^2 = |<0|X|n>|^2 = \frac{e^{-\lambda^2}\lambda^{2n}}{n!} \qquad (1)$$

between a state with 0 phonons and a state with n phonons where λ is the electron-phonon coupling strength, also called the Huang-Rhys factor.

In bulk PbS, the energy of the zero-wave-vector (Γ-point) transverse-optical phonon is 8.1 meV as observed through far-infrared absorption[42] spectroscopy and Raman spectroscopy[43, 44]. Furthermore, vibronic quantum beats have also been observed in femtosecond optical spectroscopy[44, 45] of PbS QDs.

Phonon modes can also be observed in the inelastic ETS[46]. These low energy modes could be not be observed in samples A and B because of the Coulomb gap at low bias. However, one of the studied sample was in the regime of shell-tunneling and, consequently, did not present Coulomb blockade effects, Fig. 5a. The absence of the sharp Coulomb blockade peaks does not allow the observation of the phonon sub-bands, however, the absence of the gap at zero bias allows measurements of the inelastic ETS d^2I/dV^2, shown Fig. 5b. This last spectrum shows the first three optical phonon modes at the

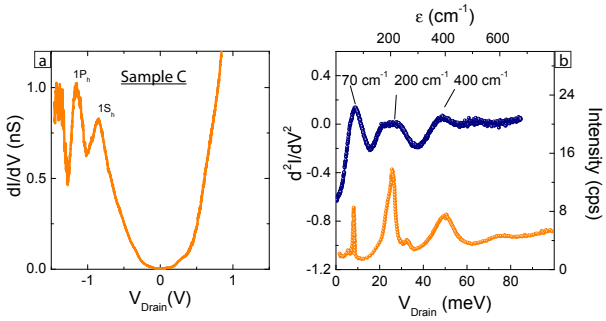

FIG. 5. (a) dI/dV curves for sample C showing the excited hole levels, 1Sh, 1Ph, measured at $T = 5\ K$. Note the absence of the Coulomb peaks in this shell-tunneling regime. (b) Inelastic ETS d^2I/dV^2 showing three lowest phonons mode compared to the Raman spectrum extracted from Ref.[43].

position expected from Raman spectroscopy[43].

Returning to samples A and B, one observe, Fig. 3ab and Fig. 4ab, respectively, that a gap remains at low bias at any gate voltage. Given the signature of strong electron-phonon coupling observed in these PbS QDs, a FC blockade could be at the origin of this low bias suppression of conductance[47, 48]. While the Coulomb blockade can always be lifted at appropriate gate voltage values, the FC blockade cannot be lifted by a gate bias, which is a distinguishing feature of the FC blockade. This FC blockade has also been observed in carbon nanotube based QDs[40, 41]. The FC blockade originates from the behavior of the FC matrix element X_{0n}. When tunneling on the QD, the electron shifts the equilibrium coordinate of the QD by an amount proportional to the Huang-Rhys factor λ. As the overlap between states of different phonons occupation is exponentially sensitive to this geometrical displacement, the ground-state to ground-state transition is exponentially suppressed for strong electron-phonon coupling.

For equilibrated phonons, this suppression dominates until the bias voltage is high enough, $eV \sim \lambda^2\hbar\omega_0$[47, 48], to escape from the blockade regime by transitions from zero phonons to highly excited phonon states. From the observed gap values for sample A (~ 25 meV) and sample B (~ 50 meV), we find that the electron-phonon coupling constant is in the range $\lambda \sim 1.7 - 2.5$, which is very large, of the order of the Huang-Rhis factor obtained from Raman scattering experiments[43]. While there is no consensus on the effects of quantum confinement on electron-phonon coupling, see. Ref. [49] for a review, it has been suggested that a large electron-phonon coupling in QDs could be the consequence of trapped charges at the surface of QDs[43] or polaronic effects that would arise as a consequence of the discrete electronic levels[50].

We thank A. Descamps-Mandine and M. Rosticher for their technical support with the SEM and the clean room work, respectively. We acknowledge support from

ANR grant "QUANTICON" 10-0409-01, ANR Grant "CAMELEON" 09-BLAN-0388-01 and Region Ile-de-France in the framework ofDIM Nano-K.

* Herve.Aubin@espci.fr

[1] A. P. Alivisatos, Science **271**, 933 (1996).

[2] C. Delerue and M. Lannoo, *Nanostructures: Theory and Modelling* (Springer, 2004) p. 304.

[3] D. V. Talapin and C. B. Murray, Science (New York, N.Y.) **310**, 86 (2005).

[4] J. J. Urban, D. V. Talapin, E. V. Shevchenko, C. R. Kagan, and C. B. Murray, Nature materials **6**, 115 (2007).

[5] Z. Chen, B. Nadal, B. Mahler, H. Aubin, and B. Dubertret, Advanced Functional Materials **24**, 295 (2014).

[6] F. W. Wise, Accounts of chemical research **33**, 773 (2000).

[7] G. Konstantatos, I. Howard, A. Fischer, S. Hoogland, J. Clifford, E. Klem, L. Levina, and E. H. Sargent, Nature **442**, 180 (2006).

[8] V. I. Klimov, Annual review of physical chemistry **58**, 635 (2007).

[9] A. Pandey and P. Guyot-Sionnest, Science (New York, N.Y.) **322**, 929 (2008).

[10] E. Lhuillier, A. Robin, S. Ithurria, H. Aubin, and B. Dubertret, Nano letters **14**, 2715 (2014).

[11] W. K. Koh, S. R. Saudari, A. T. Fafarman, C. R. Kagan, and C. B. Murray, Nano Letters **11**, 4764 (2011).

[12] A. Nag, M. V. Kovalenko, J.-s. Lee, W. Liu, B. Spokoyny, and D. V. Talapin, Journal of the American Chemical Society **133**, 10612 (2011).

[13] O. Millo, D. Katz, Y. Cao, and U. Banin, Physical Review B **61**, 16773 (2000).

[14] O. Millo, D. Katz, Y. Cao, and U. Banin, Physical Review Letters **86**, 5751 (2001).

[15] U. Banin, Y. Cao, D. Katz, and O. Millo, Nature **400**, 5 (1999).

[16] T. Maltezopoulos, A. Bolz, C. Meyer, C. Heyn, W. Hansen, M. Morgenstern, and R. Wiesendanger, Physical Review Letters **91**, 2 (2003).

[17] T. Wang, R. Vaxenburg, W. Liu, S. M. Rupich, E. Lifshitz, A. L. Efros, D. V. Talapin, S. J. Sibener, and W. E. T. Al, (2014).

[18] P. Liljeroth, P. van Emmichoven, S. Hickey, H. Weller, B. Grandidier, G. Allan, and D. Vanmaekelbergh, Physical Review Letters **95**, 1 (2005).

[19] E. P. A. M. Bakkers, Z. Hens, A. Zunger, A. Franceschetti, L. P. Kouwenhoven, L. Gurevich, and D. Vanmaekelbergh, Nano Letters **1**, 551 (2001).

[20] L. Jdira, K. Overgaag, J. Gerritsen, D. Vanmaekelbergh, P. Liljeroth, and S. Speller, Nano letters **8**, 4014 (2008).

[21] Z. Sun, I. Swart, C. Delerue, D. Vanmaekelbergh, and P. Liljeroth, Physical Review Letters **102**, 196401 (2009).

[22] B. Diaconescu, L. a. Padilha, P. Nagpal, B. S. Swartzentruber, and V. I. Klimov, Physical Review Letters **110**, 127406 (2013).

[23] Z. Hens, D. Vanmaekelbergh, E. Stoffels, and H. van Kempen, Physical Review Letters **88**, 1 (2002).

[24] D. L. Klein, R. Richard, K. L. Andrew, a. P. Alivisatos, and P. L. Mceuen, Nature **323**, 699 (1997).

[25] F. Kuemmeth, K. I. Bolotin, S.-F. Shi, and D. C. Ralph, Nano letters **8**, 4506 (2008).

[26] Q. Yu, A. Mottaghizadeh, H. Wang, C. Ulysse, A. Zimmers, V. Rebuttini, N. Pinna, and H. Aubin, Physical Review B **90**, 075122 (2014).

[27] Q. Yu, L. Cui, N. Lequeux, A. Zimmers, C. Ulysse, V. Rebuttini, N. Pinna, and H. Aubin, ACS nano **7**, 1487 (2013).

[28] L. Jdira, K. Overgaag, R. Stiufiuc, B. Grandidier, C. Delerue, S. Speller, and D. Vanmaekelbergh, Physical Review B **77**, 1 (2008).

[29] G. a. Grinbom, M. Saraf, C. Saguy, A. C. Bartnik, F. Wise, and E. Lifshitz, Physical Review B **81**, 1 (2010).

[30] Y. Niquet, C. Delerue, G. Allan, and M. Lannoo, Physical Review B **65**, 165334 (2002).

[31] "See Supplementary Information,".

[32] I. Kang and F. W. Wise, Journal of the Optical Society of America B **14**, 1632 (1997).

[33] L. P. Kouwenhoven, D. G. Austing, and S. Tarucha, Reports on Progress in Physics **64**, 701 (2001).

[34] P. Nagpal and V. I. Klimov, Nature communications **2**, 486 (2011).

[35] N. S. Wingreen and J. W. Wilkins, Physical Review B **40**, 11834 (1989).

[36] A. Mitra, I. Aleiner, and A. J. Millis, Physical Review B **69**, 245302 (2004).

[37] J. Park, H. Park, A. Lim, E. Anderson, A. Alivisatos, and P. McEuen, Nature **407**, 57 (2000).

[38] R. H. M. Smit, Y. Noat, C. Untiedt, N. D. Lang, M. C. van Hemert, and J. M. van Ruitenbeek, Nature **419**, 906 (2002).

[39] X. H. Qiu, G. V. Nazin, and W. Ho, Physical Review Letters **92**, 206102 (2004).

[40] S. Sapmaz, P. Jarillo-Herrero, Y. Blanter, C. Dekker, and H. van der Zant, Physical Review Letters **96**, 026801 (2006).

[41] R. Leturcq, C. Stampfer, K. Inderbitzin, L. Durrer, C. Hierold, E. Mariani, M. G. Schultz, F. von Oppen, and K. Ensslin, Nature Physics **5**, 327 (2009).

[42] T. Krauss, F. Wise, and D. Tanner, Physical review letters **76**, 1376 (1996).

[43] T. D. Krauss and F. W. Wise, Physical Review B **55**, 9860 (1997).

[44] T. Krauss and F. Wise, Physical Review Letters **79**, 5102 (1997).

[45] J. Bylsma, P. Dey, J. Paul, S. Hoogland, E. H. Sargent, J. M. Luther, M. C. Beard, and D. Karaiskaj, Physical Review B **86**, 125322 (2012).

[46] P. K. Hansma, *Tunneling Spectroscopy: Capabilities, Applications, and New Techniques*, Vol. 9 (Plenum Press, 1982) p. 493.

[47] J. Koch and F. von Oppen, Physical Review Letters **94**, 206804 (2005).

[48] J. Koch, F. von Oppen, and a. Andreev, Physical Review B **74**, 205438 (2006).

[49] D. Sagar, R. Cooney, S. Sewall, E. Dias, M. Barsan, I. Butler, and P. Kambhampati, Physical Review B **77**, 235321 (2008).

[50] R. Ferreira, O. Verzelen, and G. Bastard, Physical Review Letters **88**, 146803 (2002).